Retinal Vascular Branching in Healthy and Diabetic Subjects

Ting Luo, Thomas J. Gast, Tyler J. Vermeer, and Stephen A. Burns

School of Optometry, Indiana University, Bloomington, Indiana, United States

PURPOSE. To measure the effect of nonproliferative diabetic retinopathy (NPDR) on retinal branching. To compare vascular branching in healthy and diabetic subjects with established biophysical models.

METHODS. Vascular bifurcations in arteries and veins were imaged in 17 NPDR and 26 healthy subjects with the Indiana adaptive optics scanning laser ophthalmoscope (AOSLO). Vessel measurements were grouped according to parent vessel diameters into large ($\leq$50 ~ <100 μm) and small ($\leq$20 ~ <50 μm) sizes. Vessel diameters and bifurcation angles were measured manually. Vascular diameters were compared with predictions of Murray's law using curve fitting. For analysis of bifurcation angles, two models from Zamir were compared: one based on the power required for blood pumping, the other based on drag force between blood and vascular wall.

RESULTS. For normal larger vessels, the exponent relating the parent and daughter branching diameters was significantly less than the value of 3 predicted by Murray's law (arteries: 2.59; veins: 1.95). In NPDR, the best-fit exponent was close to 3 for arteries but close to 2 in healthy subjects in veins, (arteries: 3.09; veins: 2.16). For both small arteries and veins, diabetics' exponent differed from healthy subjects ($P < 0.01$). Bifurcation angles in the healthy subjects (78° $\pm$ with a standard error (SE) of 0.9°) were not much different than in NPDR (79° $\pm$ SE 1.3°). The model based on minimizing pumping power predicted the measurements better than the one minimizing the vascular drag and lumen surface area.

CONCLUSIONS. The relation between parent and daughter branch diameters changes in diabetes, but the branching angles do not.

Keywords: vascular branching, Murray's law, adaptive optics scanning laser ophthalmoscopy, diabetic retinopathy

Diabetes is a group of metabolic diseases that affects approximately 150 million people worldwide, and this number is predicted to double by the year 2025.[1] Diabetes affects multiple organs throughout body, including the eye. When it affects the retina of the eye it produces diabetic retinopathy (DR), which is the leading cause of blindness in working age adults,[2] affecting 40% to 45% of the diabetic population.[1] The prevalence of DR increases with the duration of diabetes. For those with a duration of less than 5 years, the prevalence of DR is less than 10%, and this percentage increases to approximately 50% with a 20-year history of diabetes.[3]

Many of the retinal complications of diabetes arise from its impact on retinal blood vessels, including changes to the retinal vascular architecture,[4] tortuosity[5,6] retinal vascular branching diameter,[5,7–10] and branching angle.[6] Some of these early changes are associated with a risk for progression to more serious stages of DR.[11] The vascular remodeling in diabetes is of interest because there are well-developed biophysical models of the geometry of vascular branching. The best known of these is Murray's law.[12] Murray derived the expected relation in a branching network between the diameter of a parent vessel and the daughter vessels by minimizing a cost function that expresses the vascular resistance for a given vascular volume. The derivation includes two factors affecting cost minimization:

the energy cost associated with maintaining the vascular system, and the cost of distributing the Newtonian fluid (blood in vascular system) involved. The resulting prediction, now called Murray's law, states that the cube of the parent vessel's diameter is equal to the sum of the cubes of the daughters' diameters. For a bifurcation, the equation can be expressed as

$$P^3 = D_1^3 + D_2^3 \qquad (1)$$

where P is the parent diameter while the D_i are the daughter diameters.

Murray's analysis also leads to a prediction of the angle for a simple symmetric bifurcation of 75°.[13] This prediction confirmed Roux's previous measurement that showed a branching angle of approximately 70° (as reported by Murray[13]).

However, Murray's[13] description of the angular relations has been considered too general to be fully useful and not realistic when applied to biological systems.[14] This led to multiple refinements of Murray's law that emphasized different minimization criteria, including drag[14] and volume.[15] Zamir[16] proposed that four local parameters: minimum volume, minimum surface, minimum power expenditure, and minimum shear stress should govern the branching of blood vessels in the cardiovascular system.

Murray's power law governing parent and daughter vessel diameters has been verified in some biological system.[17–21]

Similarly, Zamir's modified prediction of the branching angles has been confirmed to some extent.[22,23] However, neither of these laws has been examined in vivo throughout the full size range of the blood vessels in the ocular vasculature. Our application of multiply scattered light adaptive optics scanning laser ophthalmoscope (AOSLO) imaging allows us to explore this relation in healthy subjects as well as in diabetic subjects where vascular alterations could change these relations.

Diabetes affects the physical properties of the blood as well as the vascular endothelium, and thus could change the biophysical relations described above. In fact, unlike results from larger vessels in the body, the results from larger retinal vessels tend to deviate from Murray's law.[24] In recent years, adaptive optics has improved the lateral resolution and accuracy of retinal imaging measurements and has been successfully used to image the retina of healthy[25] and diseased eyes.[26] Recently, the combination of adaptive optics with an aperture positioned to collect multiply scattered light by moving the aperture to block singly scattered light was shown to increase the contrast of vascular wall structures compared with the confocal setting.[27–31] We take advantage of the improved lateral resolution of AOSLO images to make more precise measurements of retinal vascular branching in healthy and diabetic subjects, refining prior studies and extending them to smaller retinal vessels. These measurements allow us to compare data over the full range of retinal vascular dimensions and to compare them with biophysical predictions.

METHODS

Subjects

Twenty six healthy subjects (38.7 years ± 13.6) and 17 nonproliferative diabetic (NPDR) patients (46.2 years ± 9.7) participated in this study. Five of 17 diabetic subjects had managed hypertension. Exclusion criteria for subjects included any retinal or systemic disease other than diabetes. Each subject first received an ophthalmic examination, including a subjective refraction and fundus exam as well as imaging using a Heidelberg OCT Spectralis (Heidelberg Engineering GmbH, Heidelberg, Germany). One eye from each subject was tested. The imaging session were conducted after the pupil was dilated with 0.5% Tropicamide.

Informed consent was obtained after a full explanation of the procedures and consequence of the study prior to participation. The protocol of this study was approved by the Indiana University institutional review board and complied with the tenets of the Declaration of Helsinki.

Imaging Method

The Indiana AOSLO system has been described previously.[32] In brief, the AOSLO uses a supercontinuum light source (SuperK Extreme; NKT Photonics, Birkerød, Denmark) for both wavefront sensing and retinal imaging. Wavefront sensing is performed at 856 nm and the two imaging beams were 820 (bandwidth: 19 nm) and 775 nm (bandwidth: 26 nm). The total light level was safe according to American National Standards Institute (ANSI Z136) standards. The system uses two deformable mirrors, a Mirao with 52 actuators (Mirao TM 52-e; Imaging Eyes, Orsay, France) to correct low-order aberrations and a Boston Micromachines Corp. mirror with 144 actuators (Multi-DM; Boston Micromachines Corporation, Cambridge, MA, USA) to correct high-order aberrations. The two mirrors operating in a woofer tweeter configuration.[33] Two scanners are used to create the raster on the retina. The horizontal scanner works at a frequency of 16 kHz and the vertical scanner generated 520 lines giving a frame rate of approximately 30 frames per second. The standard imaging size is approximately 1.8° × 1.9°, which corresponds to a retinal region of approximately 520 × 550 μm. The lateral resolution of the system is approximately 2 μm with an 8-mm pupil. The imaging field could be steered across the retina through a 30° angle.[32,34]

Multiply Scattered Light Imaging

For the current study, we used two different imaging channels to simultaneously generate a confocal and a multiply scattered light image. A ×2 Airy disk diameter aperture was used to obtain confocal images in the confocal channel, and a ×10 Airy disk diameter aperture offset at least ×6 Airy disk diameters was used to obtain multiply scattered light images of the vasculature. The direction of the displacement was varied depending on the orientation of the blood vessel in order to maximize contrast.[28] During imaging, the operator made real-time adjustments to focus and aperture offset to optimize images.[31]

Imaging Acquisition and Processing

Adaptive optics scanning laser ophthalmoscope images were recorded as a series of videos in each location for approximately 3.3 seconds (100 frames). The imaging distortions created by the sinusoidal horizontal scan were corrected before frame alignment. Then, the aligning and averaging of the frames was performed by using a custom Matlab (Mathworks, Natick, MA, USA) routine. A template frame was automatically selected based on brightness and cross-correlation value compared with the previous frame. Each individual frame in the video was then aligned to the selected template, rejecting frames with large eye movement or blinks. After that, the final alignment is created based on determining the eye movements using stripwise cross-correlation.[35,36] Because images from both confocal and offset channels are captured simultaneously, the corrections needed to align the frames of the videos and remove eye movement, were calculated using the images from the confocal channel and were applied to the multiply scattered light channel. The customized program then generated aligned video sequences and averaged images using 'lucky averaging' to optimize the final imaging quality.[37] From the averaged images, bifurcations were then selected for measurement. Inclusion criteria for the analysis of lumen diameter included: (1) sufficient image quality for visualizing the lumen of the vessel, (2) excluding parent lumen diameters less than 20 μm, and (3) excluding daughter lumen diameters less than 8 μm, because these measurements were less accurate due to pixelation.

Imaging of Retinal Vasculature Branching

Adaptive optics scanning laser ophthalmoscope imaging was started close to the optic nerve and then following an artery temporally, imaging bifurcations along both the superior and inferior arcades. Imaging proceeded from large vessels to small, and then returned along venules and veins toward the optic nerve. The operator was aided by a fundus photo with a superimposed square indicating the current imaging location that was visualized in real time during AOSLO imaging. Subjects fixated a target provided by an auxiliary fixation system while the operator steered the imaging field. Adaptive optics scanning laser ophthalmoscope imaging sessions required approximately 30 minutes to image 15 to 20 blood vessel bifurcations for each subject. For subjects having a sufficient number of bifurcations, 15 to 20 bifurcations were
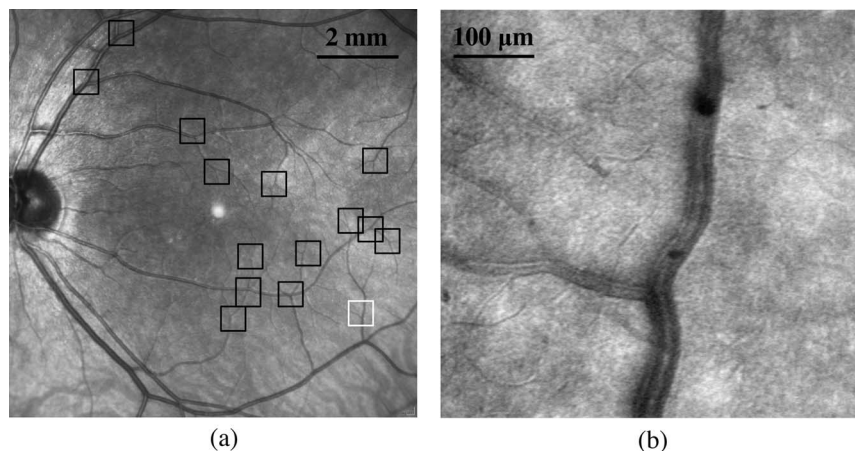
FIGURE 1. (**a**) Example of a fundus picture with AOSLO sampling locations indicated (*black boxes*). (**b**) Example of AOSLO image of small veins used for branching measurement in this subject from the *white box* in (**a**).

randomly chosen along both superior and inferior arcades and imaged. For subjects with fewer bifurcations, all bifurcations along the selected vessels were imaged. We imaged vascular branches on arteries and veins whose diameter ranged from 7 to 150 μm (exclusion criteria mentioned above applied later during measurements). Cilioretinal vessels were avoided. Figure 1 shows the fundus picture of one subject captured using the Spectralis SLO with boxes indicating where bifurcations were imaged. The AOSLO imaged bifurcation in Figure 1b is marked as the white box (Fig. 1a).

Data Analysis

For each bifurcation, the lumen diameter was measured at one parent diameter distance from the bifurcation point. The measurements were repeated five times for the parent as well as for each of the daughter branches. Each of the five measurements was separated by approximately 10 to 12 μm. The diameter and the angles of each bifurcation were measured with Adobe Photoshop CS6 Extended (Adobe System, Inc., San Jose, CA, USA). For vascular diameter measurements, only multiply scattered light images were used. For the branching angles analysis, both multiply scattered light images and perfusion maps (based on the standard error of

multiply scattered light images) were used (Fig. 2). However, because the multiply scattered light measurements were more reliable (see validation below) only those measurements were used in the fitting of the power law to the vascular diameters. The measurement data was then exported from Photoshop to Microsoft Excel (Microsoft, Redmond, WA, USA) and Matlab for analysis.

The exponent of vascular lumen diameter was fit using the Matlab curve fitting toolbox by using the equation

$$P^a = D_1^a + D_2^a \qquad (2)$$

where the superscript "a" is the variable and P, D_1, D_2 stand for the lumen diameter of the parent vessel and the two daughter branches respectively. Subscript 1 refers to the larger of the two daughter branches and subscript 2 to the smaller daughter branch. The outputs from the fitting provided a least squares estimate of "a," as well as an estimate of the 95% confidence limits (CL) for the value of "a." The bifurcation angle θ was calculated by adding $θ_1$ and $θ_2$, which were measured at each bifurcation on both the multiply scattered light images (Fig. 3) and the perfusion maps. For each $θ_1$ and $θ_2$, the results were calculated as the average of the two forms of images. The results then were compared with predicted
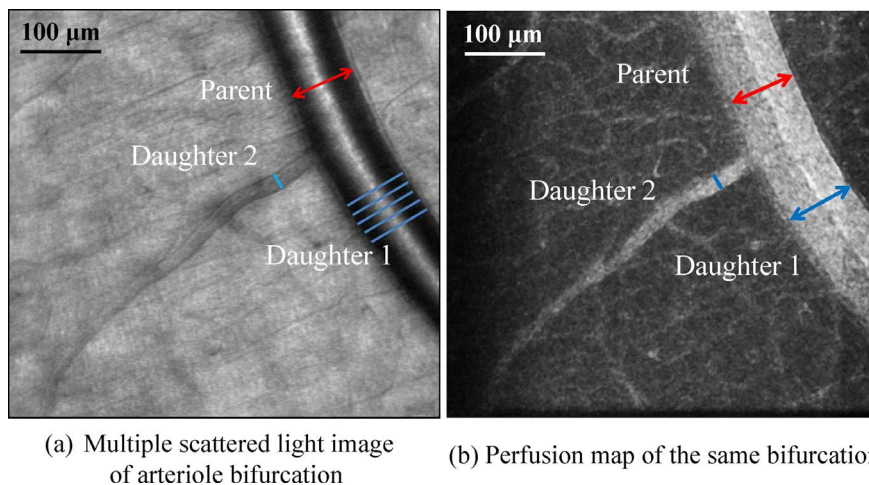
(a) Multiple scattered light image of arteriole bifurcation

(b) Perfusion map of the same bifurcation

FIGURE 2. Example of measurement technique for a single vascular bifurcation in a healthy subject. *Red arrows*, *blue arrows*, and *lines* show the diameter of parents and both daughters, respectively. Measurements of parent and daughters' diameters repeated five times starting at one parent diameter from the bifurcation point and spaced 10 to 12 μm as shown for daughter branch 1 in (**a**).
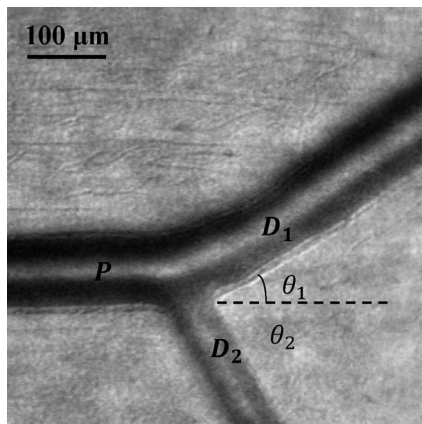
FIGURE 3. Adaptive optics scanning laser ophthalmoscope image of a retinal bifurcation with parent (P) and daughter branches (D$_1$, D$_2$, with D$_1$ being the larger of the two). Angles are measured from the extension of a line parallel to the center of the parent vessel, through the bifurcation (θ_1, θ_2). The bifurcation angle is calculated as the sum of θ_1 and θ_2.

FIGURE 4. Fitting exponent with the 95% CL for each group. The number of analyzed branches is shown at the bottom of each bar with * signifying that the means were outside the 95% CL.

theoretical values calculated from the equation derived by Zamir.[16]

Validation of the Data

For a subset of the data, two experienced graders manually performed repeated diameter measurements in two ways. The first two subjects, one diabetic and one healthy, were randomly selected and all 31 bifurcations (93 total vessels) were graded (21 from the control and 10 from the diabetic). The interclass correlation coefficient (ICC) was used to evaluate interrater reliability.[38] The one-way model ICC test was performed in Matlab and the ICC value for the control subject data was 0.985 (0.975, 0.990, 95% lower and upper bounds) while the ICC value for the diabetic subject was 0.969 (0.936, 0.985). In the second comparison 10 bifurcations from healthy and 13 from diabetic subjects were randomly selected from all images (giving 69 diameter measurements). The ICC value was 0.938 (0.937, 0.940) for the control and 0.938 (0.937, 0.939) for the diabetic group. Given the high ICC between the graders the main analysis was performed based on results from one grader.

Weighting of the Data

The number of bifurcations imaged for each subject differed both due to anatomic factors and image quality variations. For

TABLE 1. The Number of Bifurcations From Different Data Groups and the Best Fitting Exponent

Category (Population, Vessel Type, Size)	Best Fitting Exponent (95% CL)	Number of Vascular Branches Analyzed
Healthy, artery, small	2.10 (1.92, 2.28)	73
Healthy, artery, large	2.74 (2.49, 2.94)	130
Healthy, vein, small	1.69 (1.58, 1.81)	116
Healthy, vein, large	2.11 (1.79, 2.43)	23
Diabetes, artery, small	3.21 (2.32, 4.09)	35
Diabetes, artery, large	3.05 (2.47, 3.64)	36
Diabetes, vein, small	2.02 (1.75, 2.29)	40
Diabetes, vein, large	2.24 (1.71, 2.76)	11

Small, 20 μm ≤ parent diameter < 50 μm; large, 50 μm ≤ parent diameter < 100 μm.
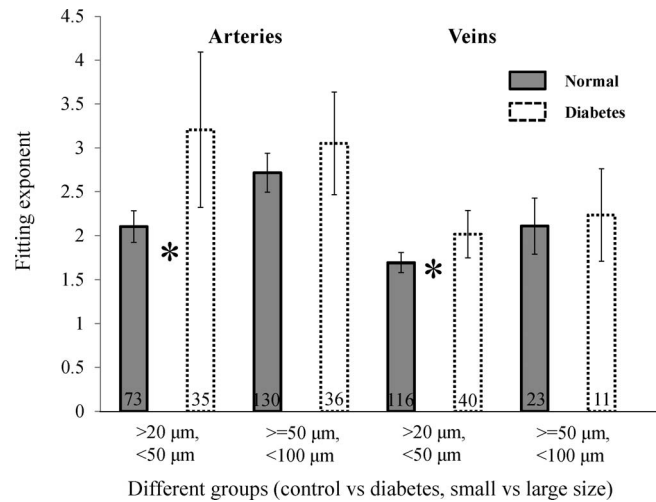
this reason the study data had unequal numbers of bifurcations per subject. To control for this potential bias when estimating the best fit parameters, we weighted each individual measurement by 1/(total number of bifurcations measured in that subject). This weighting was performed for each comparison made (according to vessel size, veins versus arteries, and healthy versus diabetic).

RESULTS

### Lumen Diameter in Parent and Daughter Branches

A total of 274 distinct artery and 190 distinct vein bifurcations were measured. Data were divided into groups based on size and artery versus vein for both healthy and diabetic subjects (Table 1).

The best-fitting exponent to Equation 2 for all data ranged from 1.7 to 3.2 (Table 1). The exponent estimates ranged from 1.6 to 4.1, and the value of 3 predicted by Murray's law fell outside the 95% CL for all of the control groups and for diabetic veins. For diabetic subjects, exponents were larger than healthy subjects (fitting exponents ranged from 2–3.2) for all vessel sizes and CL were larger (Table 1; Fig. 4). The differences was largest for comparisons of small arteries where the 95% CL did not overlap and for small veins, the means did not fall within the 95% CL. Because the diabetics had a slightly larger mean age than the healthy subjects, we also subdivided our healthy group by splitting the data at the mean age, providing subgroups with an average age of 27 and 52 years. The average exponent for the two groups was not significantly different (2.23 and 2.18, respectively), and thus we used the combined group for all other analyses.

Bifurcation Angles

We measured 342 bifurcation angles in healthy subjects and 122 bifurcation angles in NPDR subjects. The mean bifurcation angle for controls is 78° with a SE of 0.9° and a SD of 18°. The mean bifurcation angle for diabetic subject was 79° with a SE of 1.3° and a SD of 17°.

Bifurcation angles were variable at all asymmetry ratios for both healthy and diabetic subjects (Fig. 5). This variability was particularly evident when one of the branches was small relative to the parent, as seen toward the left side of the
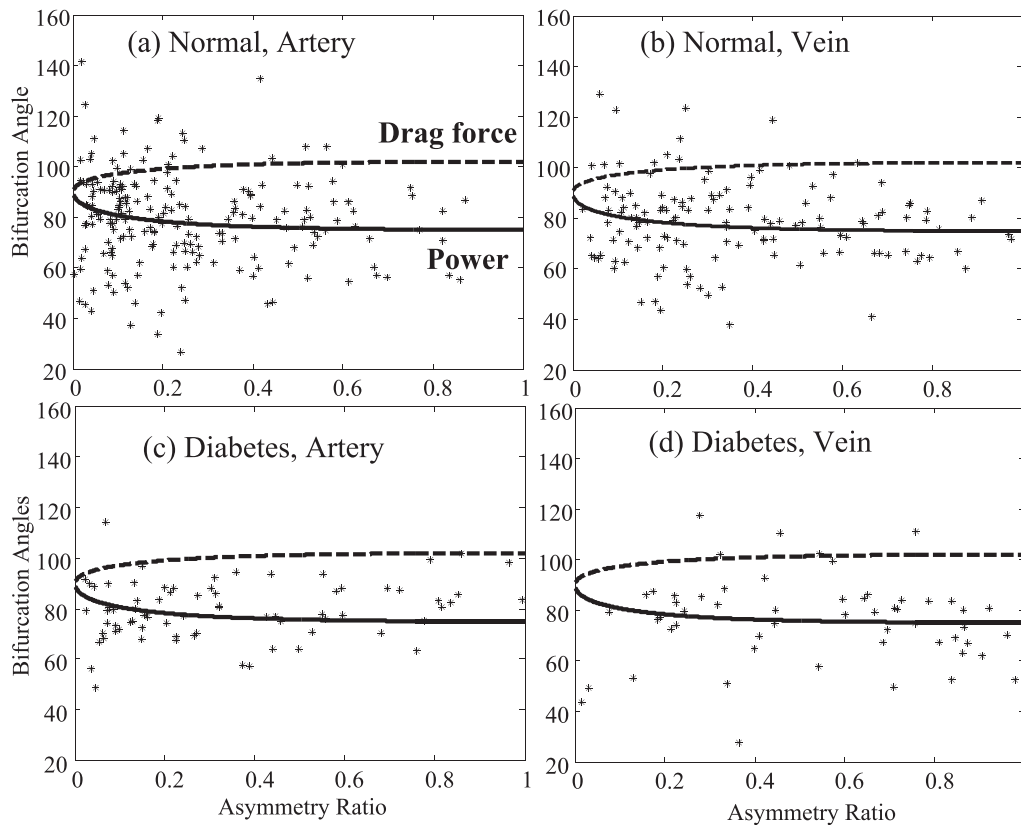
FIGURE 5. In (**a**), (**b**), (**c**), and (**d**) the *dashed black line* and *solid black line* are theoretical bifurcation range in different groups. The lower range *solid line* has been predicted by minimizing the vasculature pumping power and lumen volume. The upper range *dashed line* has been predicted by optimizing and minimizing the vasculature drag and lumen surface. *Stars*: measured angle. The horizontal axis is the ratio of the smaller daughter vessel's diameter squared to the larger daughter's diameter squared, the asymmetry ratio.

abscissa. The dependence of the bifurcation angle on the asymmetry of the daughter branches was also relatively low (Fig. 5). The two lines represent the different theoretical predictions of Zamir.[16] The two models were compared by subtracting the measured angles from the two predictions and testing whether the means differed from 0. The data were significantly different from the drag force model but not the power model for both healthy subjects ($P = 0.82$ [power model] and $P < 0.001$ [drag force model]) and for diabetics ($P = 0.97$ [power model] and $P < 0.001$ [drag force model]).

DISCUSSION

Deviation From Murray's Law

Our results in healthy subjects agree with previous studies that the exponent for parent and daughter relationships is less than 3, and thus deviate from the Murray's law prediction of 3.0. Our value for larger arteries (2.7), is in good agreement with Riva's result[39] of 2.76 and Stanton's value of 2.65.[24] Unlike Riva and Stanton, our result is not within the 95% CL of 3. Smaller

arterioles had an even smaller exponent, but these cannot be readily compared with the literature because most previous studies were restricted to vessels larger than 39 μm in diameter (Table 2). For venules, the deviation from Murray's law was even larger. The larger venules had an exponent of 2.1 and small venules had an exponent of 1.7. This is not in agreement with Riva's result because he reports a value of 2.84; however, the size of the veins Riva measured is very different from those measured in this study. Our large veins ranged from 50 to 100 μm, whereas his ranged from 64 to 177 μm, which includes the large vessels near the disk. Also the technology he used to measure vessels is quite different from the current study. Given the sharp decrease in exponent with decreasing size in both the healthy and diabetic groups (Table 1; Fig. 4), it is possible that the discrepancy arises from the sampling difference. However, in all cases for both arteries and veins, there is considerable evidence that the branching of retinal vessels does not follow Murray's law. Murray's law can hold for large vessels elsewhere in the body,[40] and it is reasonable that deviations from that law are observed for small vessels, whose diameter is closer to the size of the erythrocytes. We find the

TABLE 2. Previous Estimates of Fitting Exponent

Subjects Type	Vascular Range	Fitting Exponent	Researcher
Healthy human eye (Vein)	64–177 μm	2.84	Riva et al.[39]
Healthy human eye (artery)	39–134 μm	2.80	Riva et al.[39]
Human eye (normotensive, artery)	–	2.65	Stanton et al.[24]
Human eye (hypertensive, artery)	–	2.48	Stanton et al.[24]

TABLE 3. Compensating Coefficents and Viscosity for Different Radius Range

Radius	C	α
If r > 270 μm	2.65	3.00
If 270 μm ≥ r ≥ 45 μm	7.53	2.87
If r < 45 μm	0.41	3.66

FIGURE 6. Shows an AOSLO image of a vein. *Black arrow* shows the blood flow direction of the parent branch. Laminar flow with different layers are clearly seen in both daughter and parent branches with *dark lines* in the blood column representing plasma layers separating the fused blood flows from separate daughter branches.

smallest fitting exponents for our smallest vessels. This may be due to the relative size of parent diameter and daughter branches, as discussed in more detail below.
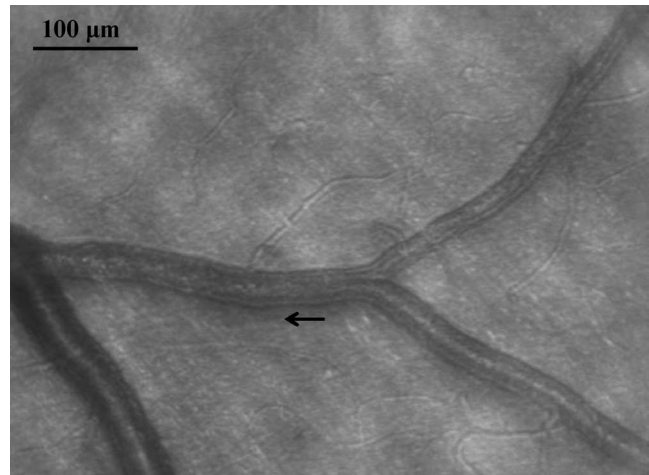
In the derivation of Murray's law, Murray treated fluids as Newtonian, and therefore the viscosity is constant and independent of vessel diameter. However, Martini,[41] and Fåhræus and Lindqvist[42] found that the viscosity of blood changes with the diameter of the tube it travels through, a property now known as the Fåhræus-Lindqvist effect. In particular, the viscosity of blood decreases relative to Newtonian viscosity, which is a constant, as a tube's diameter decreases for vessel diameters between 300 and 10 μm. For even smaller vessels (below 10 μm) the trend reverses from the Fåhræus-Lindqvist effect and viscosity increases again.[43] The Fåhræus-Lindqvist effect occurs mainly due to the tendency of erythrocytes to move toward the center of the vessel, leaving only plasma close to the vessel walls. To date, this nonlinear behavior of blood viscosity has been attributed to shear stress.[44] Theories include the intra-arterial pressure hypothesis,[45] and endothelial surface layer formation theory.[46,47] All these theories indicate that treating blood viscosity as a constant is a very crude approximation especially for blood vessels with diameters under 300 μm. Instead, viscosity needs to be treated as a variable dependent on vascular diameter. This has been examined for some nonocular vascular beds,[48] evaluating Murray's law for blood vascular systems based on Pries' assumption[49] that blood viscosity is a function of hematocrit level and the vessel radius. By assuming an approximation of hematocrit (the decimal fraction of whole blood occupied by erythrocytes) as 0.45, and adding compensating coefficients to each parent and daughter diameter Alarcond[48] derived the following relationship between parent and daughter radius:

$$C(R_p, H_p)R_p^{\alpha(R_p, H_p)} = C(R_1, H_1)R_1^{\alpha(R_1, H_1)} + C(R_2, H_2)R_2^{\alpha(R_2, H_2)}$$

(3)

where C is the compensating coefficient, α is the viscosity, and both C and α are the function of vessel radius and hematocrit level. Subscripts P, 1, and 2 stand for the parent and two daughter branches, respectively. The corresponding C and α can be found in Table 3.

Basically, Alarcon's altered Murray's law states that if the vessel radius is bigger than approximately 270 μm, then the Fåhræus-Lindqvist effect can be ignored. Treating the viscosity as a constant number is acceptable. If the vessel radius is between 270 and 45 μm, then the Fåhræus-Lindqvist effect is important and decreases blood viscosity. This decrease in viscosity changes the derivation of Murray's law because the minimization now includes a vessel size dependent viscosity, and thus decreases the exponent. When the vessel radius decreases below 45 μm, another nonlinear property of blood viscosity, the inverse Fåhræus-Lindqvist effect, yields an increase in blood viscosity and this should increases the fitting exponent again.

In our measurement, the parent diameter ranged from 20 to 100 μm. The fitting exponent of arteries from the large healthy group is 2.74, which is very close to the prediction of 2.87 by Alarcon.[48] However, Alarcon's result that increasing viscosity in smaller vessels (below 45 μm) should lead to an increase in

fitting exponent was not observed in the current study for our smaller vessel group (20 ≤ parent diameter < 50 μm). In this range, we found that the fitting exponent was smaller than for vessels larger than 50 μm. This result suggests that the cutoff vessel size in Alarcon's analysis for the reversal of the Fåhræus-Lindqvist effect may be too large. This could simply reflect the difference between the ex vivo measures of viscosity Alarcon used and the in vivo viscosity.

The exponent for the normal veins was even smaller than for the arteries. While it is not clear why the veins show this behavior, one possibility is that the pattern of laminar flow in veins is quite different than in arteries. In veins we observed that as each daughter fed into the parent the flows remain separate (Fig. 6; corresponding Supplementary Video).

This may lead to multiple plasma layers at the wall of a single vein and certainly leads to multiple streams of erythrocytes separated by plasma. This requires a larger vessel diameter, and subsequently lower velocities, and thus could generate even lower effective viscosity than in the arteries. Another consideration is that all the models of viscosity as a function of tube diameter are models of viscosity in rigid tubes, whereas the ocular vessels are pliable and elastic as can be seen on AOSLO video imaging. The impact of this lack of vessel rigidity on effective viscosity is unknown. A third possible factor affecting the exponent in veins could arise from the differences in oxygen state. Changes in oxygenation lead to changes in blood viscosity through the mechanism of erythrocytes deformability. The deformability of erythrocytes decreases significantly for deoxygenated blood.[50] However, the more increased rigidity of erythrocytes in the veins should lead to an increase in blood viscosity,[51] and thus in turn should increase, not decrease the fitting exponent in Murray's law. Thus, the lower viscosity seen in the veins are more likely to arise from their differences in erythrocyte distribution, the increased pliability of the walls, and the relatively large sizes and slower velocities.

For diabetics, the fitting exponent in arteries increased to 3.2 from the value of 2.1 seen in healthy subjects. Vascular remodeling in diabetes brings changes to vessel properties, such as diameter and increases rigidity.[52] If the net effect of these changes is to alter the vessels toward the rigid tubes on which Murray's law is based, the predicted exponent would be expected to approach 3. Additionally, serum viscosity is increased by approximately 8% in diabetes compared with

healthy subjects[53–55] and erythrocyte rigidity is also increased.[56] The decreased viscosity in small vessels due to the Fåhræus–Lindqvist effect is raised toward that seen in a Newtonian fluid by this elevation of blood viscosity in diabetes. This, in turn, could move the lower-fitting exponent seen in healthy subjects back toward Murray's prediction of 3 based on a Newtonian fluid in diabetics.

For both healthy and diabetic data, while the Fåhræus–Lindqvist effect seems to support major aspects of our results, other factors undoubtedly play a role. Those factors include the Fåhræus effect and phase separation. The Fåhræus effect is a decrease in average concentration of red blood cells (i.e., hematocrit) with decreasing diameter of the tube in which it is flowing. In other words, in blood vessels with diameters less than approximately 500 µm, the hematocrit decreases with decreasing vessel diameter. Thus, by influencing the hematocrit level, the Fåhræus effect changes the viscosity, which in turn alters the Fåhræus–Lindqvist effect. Phase separation occurs because blood plasma and erythrocytes distribute unequally at bifurcations because erythrocytes are more centrally located within the vessel. Quantitative examinations of these factors are difficult, and thus exact impacts on 4Murray's law are not available but are needed to explain the deviations from Murray's law in both healthy and diabetic subjects. Additionally, because there are not similar data for other tissues, it could be that the retina is different. One possibility is that because blood both absorbs and scatters light, the eye has other important physiological constraints in addition to energetic considerations and this could lead to larger deviations from Murray's law than are seen elsewhere in the body. That is, the requirement of minimal interference with vision, could evolutionarily trump the systemic energetic burden issues in a small essential structure.

Branching Angles

Distributing blood across a vascular network requires energy, and thus the branching pattern ideally reflects a balance between the physical energy the body expends to move blood through the network and the need for local delivery. Thus, the pattern of bifurcations should reflect a configuration that minimizes energy expenditure as discussed above. Murray[13] concentrated his analysis on the general energetic constraints while Zamir[14] analyzed two cases involving different local factors. For the first case, Zamir considered the total volume of the vessel and computed the power required to pump blood through that junction. Minimizing that power resulted in the prediction of Equation 4 (referred to as the power equation).

$$\cos\theta_1 = \frac{(1+\alpha^{3/2})^{4/3}+1-\alpha^2}{2(1+\alpha^{3/2})^{2/3}};$$

$$\cos\theta_2 = \frac{(1+\alpha^{3/2})^{4/3}+\alpha^2-1}{2\alpha(1+\alpha^{3/2})^{2/3}}. \quad (4)$$

For the second case, Zamir considered the total drag force of the blood across the total lumen surface area of the vessels. Minimizing the drag force results in the prediction of Equation 5 (referred to as the drag force equation).

$$\cos\theta_1 = \frac{(1+\alpha^{3/2})^{2/3}+1-\alpha}{2(1+\alpha^{3/2})^{1/3}};$$

$$\cos\theta_2 = \frac{(1+\alpha^{3/2})^{2/3}+\alpha-1}{2\alpha^{1/2}(1+\alpha^{3/2})^{1/3}} \quad (5)$$

α is the 'asymmetry ratio' which equal $\frac{r_2^2}{r_1^2}$ $(r_1 \geq r_2)$, this is the ratio of the cross-sectional area of the smaller branch divided by that of the larger (π cancels out), θ_1 and θ_2 are as in Figure 3.

The two general rules revealed by these qualitative results are: (1) when an artery gives rise to a relatively small branch, the angle of that branch will be close to a right angle and the parent will continue without obvious change in both size and direction; and (2) when an artery undergoes a more nearly equal bifurcation, the larger branch will make a smaller angle with the direction of the parent artery than will the smaller branch.[16]

These two equations predict the curves plotted in Figure 5, with the upper curve representing the drag force equation (dotted line) and the power equation the lower curve (solid line). We calculated the distance between our data and the theoretical predictions. The minimum pumping power prediction is a better fit, although clearly neither model is capturing the variance of the results suggesting that other factors, perhaps local anatomic factors during development, play an important role in determining vascular branching angles adding to the variability.

There was not a difference in the branching angles between control and diabetic subjects. The small measured difference in branching angle in diabetes is consistent with other studies.[21,23,57] We did observe that diabetic subjects seemed to have a relative paucity of smaller asymmetry ratios compared with our healthy subjects for the smaller arteries. To analyze this we fit the probability density for asymmetry ratios (Fig. 7) using the Beta function. The fitting parameters 'a' and 'b' are also given in Figure 7.

These apparent differences for the small diabetic arteries was confirmed by analyzing the distribution using a Wilcoxon rank sum test, a nonparametric estimate of the median, between control and NPDR groups, with the data split according to size. For small arteries and veins, the median values are different ($P < 0.01$), implying that the probability density of the asymmetry ratio is significantly different between control and NPDR groups. However, for the larger arteries and veins, the data do not support a difference between the controls and the NPDR subjects. This suggests that the diabetics are either undergoing remodeling of the small vessels or a subset of bifurcations have been lost due to capillary nonperfusion. Either way, the structure of bifurcations of the larger vessels is remaining relatively stable to within the limits of detection.

Limitations of the Current Study

Hypertension is about twice as common in diabetics as in nondiabetics,[58] and this could have impacted our results due to the effect of hypertension on retinal vessels. However, Stanton[24] showed that fitting exponents were similar for normotensives and hypertensives suggesting that this is not a likely cause of our differences between healthy and diabetic subjects. Biopsy has also shown little impact of diabetic hypertension on small artery morphology.[59] To check whether our data were impacted by including hypertensive diabetics, we omitted the five hypertensive diabetic subjects from our group of 17 diabetics. The best-fitting exponent was close to the results shown in Table 1. The differences of fitting exponent between diabetic and healthy subjects remained statistically significant for small arteries and veins ($P < 0.02$ for each), which is consistent with the results shown in Figure 4.

We also examined the probability density of the number of bifurcations according to asymmetry ratio. No obvious change of the pattern was seen when compared with Figure 6. ANOVA and post hoc Wilcoxon rank sum test were also performed. No results were changed, and thus we conclude that the main
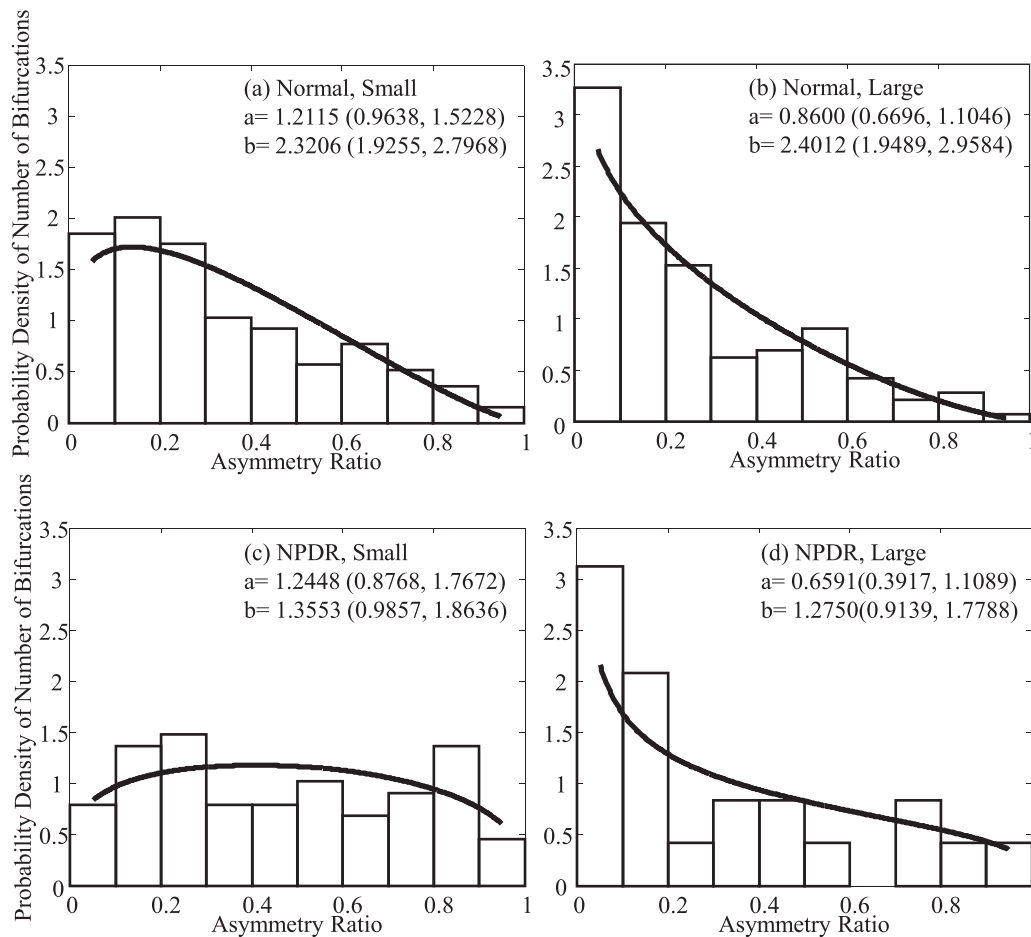
Investigative Ophthalmology & Visual Science

FIGURE 7. The probability density of the number of bifurcations according to asymmetry ratio in different groups. *Black lines* are the Beta fitting. This illustrates the relative paucity of low asymmetry ratios observed in smaller arteries for the diabetic subjects.

effects we are measuring are due to diabetes and not a comorbidity arising from hypertension.

CONCLUSIONS

Our results suggest that there is significant vascular remodeling in retinal vascular bifurcations in both mild and moderate nonproliferative diabetics. These vascular changes in diabetics involve alterations in branch diameters toward the predictions of Murray's Law possibly secondary to increased blood viscosity. Because vascular branching is thought to be sensitive to properties related to shear stress, which in turn depends on the properties of the cellular elements of the blood and flow on the endothelium, measurement of vascular branching may be a potential long-term biomarker of alterations in the diabetic vasculature.

References

1. Centers for Disease Control and Prevention. National Diabetes Fact Sheet, 2011. Available at https://www.cdc.gov/diabetes/pubs/pdf/ndfs_2011.pdf.

2. Roodhooft JM. Leading causes of blindness worldwide. *Bull Soc Belge Ophtalmol*. 2002;19–25.

3. Tapp RJ, Shaw JE, Harper CA, et al. The prevalence of and factors associated with diabetic retinopathy in the Australian population. *Diabetes Care*. 2003;26:1731–1737.

4. Ikram MK, Cheung CY, Lorenzi M, et al. Retinal vascular caliber as a biomarker for diabetes microvascular complications. *Diabetes Care*. 2013;36:750–759.

5. Cheung CY, Tay WT, Mitchell P, et al. Quantitative and qualitative retinal microvascular characteristics and blood pressure. *J Hypertens*. 2011;29:1380–1391.

6. Sasongko MB, Wang JJ, Donaghue KC, et al. Alterations in retinal microvascular geometry in young type 1 diabetes. *Diabetes Care*. 2010;33:1331–1336.

7. Nguyen TT, Wang JJ, Sharrett AR, et al. Relationship of retinal vascular caliber with diabetes and retinopathy: the multi-ethnic study of atherosclerosis (MESA). *Diabetes Care*. 2008; 31:544–549.

8. Jeganathan VS, Sabanayagam C, Tai ES, et al. Retinal vascular caliber and diabetes in a multiethnic Asian population. *Microcirculation*. 2009;16:534–543.

9. Klein R, Klein BE, Moss SE, Wong TY. Retinal vessel caliber and microvascular and macrovascular disease in type 2

diabetes: XXI: the Wisconsin epidemiologic study of diabetic retinopathy. *Ophthalmology*. 2007;114:1884–1892.

10. Klein R, Klein BE, Moss SE, Wong TY, Sharrett AR. Retinal vascular caliber in persons with type 2 diabetes: the Wisconsin epidemiological study of diabetic retinopathy: XX. *Ophthalmology*. 2006;113:1488–1498.

11. Rogers SL, Tikellis G, Cheung N, et al. Retinal arteriolar caliber predicts incident retinopathy: the Australian diabetes, obesity and lifestyle (AusDiab) study. *Diabetes Care*. 2008;31:761–763.

12. Murray CD. The physiological principle of minimum work: I. the vascular system and the cost of blood volume. *Proc Natl Acad Sci U S A*. 1926;12:207–214.

13. Murray CD. The physiological principle of minimum work applied to the angle of branching of arteries. *J Gen Physiol*. 1926;9:835–841.

14. Zamir M. The role of shear forces in arterial branching. *J Gen Physiol*. 1976;67:213–222.

15. Kamiya, Togawa. Optimal branching structure of the vascular tree. *Bull Math Biophys*. 1972;34:431–438.

16. Zamir M. Optimality principles in arterial branching. *J Theor Biol*. 1976;62:227–251.

17. Lee JY, Lee SJ. Murray's law and the bifurcation angle in the arterial micro-circulation system and their application to the design of microfluidics. *Microfluidic Nanofluidics*. 2010;8:85–95.

18. Witt NW, Chapman N, Thom SA, Stanton AV, Parker KH, Hughes AD. A novel measure to characterise optimality of diameter relationships at retinal vascular bifurcations. *Artery Res*. 2010;4:75–80.

19. Zamir M, Wrigley SM, Langille BL. Arterial bifurcations in the cardiovascular system of a rat. *J Gen Physiol*. 1983;81:325–335.

20. Zamir M, Medeiros JA, Cunningham TK. Arterial bifurcations in the human retina. *J Gen Physiol*. 1979;74:537–548.

21. Zamir M, Brown N. Arterial branching in various parts of the cardiovascular system. *Am J Anat*. 1982;163:295–307.

22. Al-Diri B, Hunter A. Automated measurements of retinal bifurcations. *IFMBE Proc*. 2009;25/11:205–208.

23. Al-Diri B, Hunter A, Steel D, Habib M. Manual measurement of retinal bifurcation features. *Conf Proc IEEE Eng Med Biol Soc*. 2010;2010:4760–4764.

24. Stanton AV, Wasan B, Cerutti A, et al. Vascular network changes in the retina with age and hypertension. *J Hypertens*. 1995;13:1724–1728.

25. Liang J, Williams DR, Miller DT. Supernormal vision and high-resolution retinal imaging through adaptive optics. *J Opt Soc Am A Opt Image Sci Vis*. 1997;14:2884–2892.

26. Roorda A. Adaptive optics ophthalmoscopy. *J Refract Surg*. 2000;16:S602–S607.

27. Elsner AE, Miura M, Burns SA, et al. Multiply scattered light tomography and confocal imaging: detecting neovascularization in age-related macular degeneration. *Opt Express*. 2000;7:95–106.

28. Chui TYP, VanNasdale DA, Burns SA. The use of forward scatter to improve retinal vascular imaging with an adaptive optics scanning laser ophthalmoscope. *Biomed Opt Express*. 2012;3:2537–2549.

29. Burns SA, Elsner AE, Chui TY, et al. In vivo adaptive optics microvascular imaging in diabetic patients without clinically severe diabetic retinopathy. *Biomed Opt Express*. 2014;5:961–974.

30. Sulai YN, Scoles D, Harvey Z, Dubra A. Visualization of retinal vascular structure and perfusion with a nonconfocal adaptive optics scanning light ophthalmoscope. *J Opt Soc Am A Opt Image Sci Vis*. 2014;31:569–579.

31. Hillard JG, Gast TJ, Chui TY, Sapir D, Burns SA. Retinal arterioles in hypo-, normo-, and hypertensive subjects measured using adaptive optics. *Trans Vis Sci Tech*. 2016;5(4):16.

32. Ferguson RD, Zhong Z, Hammer DX, et al. Adaptive optics scanning laser ophthalmoscope with integrated wide-field retinal imaging and tracking. *J Opt Soc Am A Opt Image Sci Vis*. 2010;27:A265–A277.

33. Zou W, Qi X, Burns SA. Woofer-tweeter adaptive optics scanning laser ophthalmoscopic imaging based on Lagrange-multiplier damped least-squares algorithm. *Biomed Opt Express*. 2011;2:1986–2004.

34. Huang G, Qi XF, Chui TYP, Zhong ZY, Burns SA. A clinical planning module for adaptive optics SLO imaging. *Optom Vis Sci*. 2012;89:593–601.

35. Stevenson SB, Roorda A. Correcting for miniature eye movements in high resolution scanning laser ophthalmoscopy. In: Ophthalmic Technologies XV. *Proc SPIE Int Soc Opt Eng*. 2005;5688:145–151.

36. Stetter M, Sendtner RA, Timberlake GT. A novel method for measuring saccade profiles using the scanning laser ophthalmoscope. *Vision Res*. 1996;36:1987–1994.

37. Huang G, Zhong Z, Zou W, Burns SA. Lucky averaging: quality improvement of adaptive optics scanning laser ophthalmoscope images. *Opt Lett*. 2011;36:3786–3788.

38. KO McGraw SW. Forming inferences about some intraclass correlation coefficients. *Psycholological Methods*. 1996;1:30–46.

39. Riva CE, Grunwald JE, Sinclair SH, Petrig BL. Blood velocity and volumetric flow rate in human retinal vessels. *Invest Ophthalmol Vis Sci*. 1985;26:1124–1132.

40. Sherman TF. On connecting large vessels to small. The meaning of Murray's law. *J Gen Physiol*. 1981;78:431–453.

41. Martini P, Pierach A, Schreyer E. Die Strömung des Blutes in engen Gefäßen. Eine Abweichung vom Poiseuille'schen Gesetz [in German]. *Dt Arch Klin Med*. 1930;169:212–222.

42. Fahraeus R, Lindqvist T. The viscosity of the blood in narrow capillary tubes. *Am J Physiol*. 1931;96:562–568.

43. Gaehtgens P, Duhrssen C, Albrecht KH. Motion, deformation, and interaction of blood-cells and plasma during flow through narrow capillary tubes. *Blood Cells*. 1980;6:799–812.

44. Pries AR, Schonfeld D, Gaehtgens P, Kiani MF, Cokelet GR. Diameter variability and microvascular flow resistance. *Am J Physiol Heart Circ Physiol*. 1997;272:H2716–H2725.

45. Snow HM, Mcauliffe SJG, Moors JA, Brownlie R. The relationship between blood-flow and diameter in the iliac artery of the anesthetized dog - the role of endothelium-derived relaxing factor and shear-stress. *Exp Physiol*. 1994;79:635–645.

46. Pries AR, Secomb TW, Jacobs H, Sperandio M, Osterloh K, Gaehtgens P. Microvascular blood flow resistance: role of endothelial surface layer. *Am J Physiol Heart Circ Physiol*. 1997;273:H2272–H2279.

47. Pries AR, Secomb TW. Microvascular blood viscosity in vivo and the endothelial surface layer. *Am J Physiol Heart Circ Physiol*. 2005;289:H2657–H2664.

48. Alarcon T, Byrne HM, Maini PK. A design principle for vascular beds: the effects of complex blood rheology. *Microvasc Res*. 2005;69:156–172.

49. Pries AR, Neuhaus D, Gaehtgens P. Blood-viscosity in tube flow - dependence on diameter and hematocrit. *Am J Physiol*. 1992;263:H1770–H1778.

50. Uyuklu M, Meiselman HJ, Baskurt OK. Effect of hemoglobin oxygenation level on red blood cell deformability and aggregation parameters. *Clin Hemorheol Microcirc*. 2009;41:179–188.

51. Schmidschonbein H, Wells R, Goldstone J. Influence of deformability of human red cells upon blood viscosity. *Circ Res*. 1969;25:131–143.

Investigative Ophthalmology & Visual Science

52. Zieman SJ, Melenovsky V, Kass DA. Mechanisms, pathophysiology, and therapy of arterial stiffness. *Arterioscler Thromb Vasc Biol*. 2005;25:932–943.

53. Mcmillan DE. Further observations on serum viscosity changes in diabetes mellitus. *Metabolism*. 1982;31:274–278.

54. Mcmillan DE. Disturbance of serum viscosity in diabetes-mellitus. *J Clin Invest*. 1974;53:1071–1079.

55. Mcmillan DE. The effect of diabetes on blood-flow properties. *Diabetes*. 1983;32:56–63.

56. Agrawal R, Smart T, Nobre-Cardoso J, et al. Assessment of red blood cell deformability in type 2 diabetes mellitus and diabetic retinopathy by dual optical tweezers stretching technique. *Sci Rep*. 2016;6;15873.

57. Kassab GS, Fung YC. The pattern of coronary arteriolar bifurcations and the uniform shear hypothesis. *Ann Biomed Eng*. 1995;23:13–20.

58. Sowers JR, Epstein M, Frohlich ED. Diabetes, hypertension, and cardiovascular disease: an update. *Hypertension*. 2001; 37:1053–1059.

59. Rizzoni D, Porteri E, Piccoli A, et al. Structural alterations in subcutaneous small arteries of normotensive and hypertensive patients with non insulin dependent diabetes mellitus. *Hypertension*. 1998;32:805–805.